The effect of undetected barriers on groundwater drawdown and recovery

Sarah K. Marshall

National Centre of Groundwater Research and Training (NCGRT), College of Science and Engineering, Flinders University, GPO Box 2100, Adelaide SA, 5001, Australia. Email: sarah.marshall@flinders.edu.au.

Peter G. Cook

National Centre of Groundwater Research and Training (NCGRT), College of Science and Engineering, Flinders University, GPO Box 2100, Adelaide SA, 5001, Australia. Email: peter.cook@flinders.edu.au.

Anthony D. Miller

Discipline of Mathematics, College of Science and Engineering, Flinders University, GPO Box 2100, Adelaide SA, 5001, Australia. Email: tony.miller@flinders.edu.au.

Craig T. Simmons

National Centre of Groundwater Research and Training (NCGRT), College of Science and Engineering, Flinders University, GPO Box 2100, Adelaide SA, 5001, Australia. Email: craig.simmons@flinders.edu.au.

Shawan Dogramaci

National Centre of Groundwater Research and Training (NCGRT), College of Science and Engineering, Flinders University, GPO Box 2100, Adelaide SA, 5001, Australia.

Rio Tinto Iron Ore, Wesley Quarter, Level 1, 93 William Street, Perth, 6000, WA, Australia. Email: Shawan.Dogramaci@riotinto.com.

Keywords: Analytical solutions; Groundwater hydraulics; Mining; Impermeable barriers.

Article Impact Statement: Barriers present outside the zone of pumping influence can significantly impact water level recovery, without being detected during pumping.

Abstract

In large-scale pumping projects, such as mine dewatering, predictions are often made about the rate of groundwater level recovery after pumping has ceased. However, these predictions may be impacted by geological uncertainty—including the presence of undetected impermeable barriers. During pumping, an impermeable barrier may be undetected if it is located beyond the maximum extent of the cone of depression; yet it may still control drawdown during the recovery phase. This has implications for regional-scale modelling and monitoring of groundwater level recovery. In this paper, non-dimensional solutions are developed to show the conditions under which a barrier may be undetected during pumping but still significantly impact groundwater level recovery. The magnitude of the impact from an undetected barrier will increase as the ratio of pumping rate to aquifer transmissivity increases. The results are exemplified for a hypothetical aquifer with an unknown barrier 3 km from a pumping well. The difference in drawdown between a model with and without a barrier may be <1 m in the ten years while pumping is occurring, but up to 50 m after pumping has ceased.

Introduction

Using numerical or analytical models to predict future groundwater levels, the core objective of many hydrogeological studies, is contingent upon geological understanding of a site. This paper discusses one aspect of geological complexity, that of impermeable barriers, due to their significance for studies of hydraulic head in regions with groundwater extraction. In this context, 'impermeable barriers' are a linear features that cut off or prevent groundwater flow (Ferris et al. 1962). Geological structures—such as faults and dykes—can be conduits, barriers, or complex conduit-barrier combinations to groundwater flow (Caine et al. 1996; Allen and Michel 1999; Babiker and Gudmundsson 2004; Bense and Person 2006). In fault

zones the permeability structure depends on the proportion of the core of the fault, which is generally of lower permeability, to the more permeable, outer damage zone (Caine et al. 1996). Other factors such as the host rock type, the regional stress regime, and mineral precipitation also play a role (Bense et al. 2013).

Under steady state flow conditions, impermeable barriers can influence the distribution of hydraulic heads (Rawling et al. 2001; Bense and Van Balen 2004; Seaton and Burbey 2005; Mayer et al. 2007; Bense et al. 2013; Gumm et al. 2016). Yet during groundwater extraction, if an impermeable barrier exists beyond the extent of the cone of depression, it will not have any effect on drawdown. At some distance away from pumping, the maximum decline in groundwater level may not occur until after pumping has ceased (e.g. Bredehoeft 2011). Then, if the cone of depression intersects an impermeable barrier, drawdown on the pumping side of the barrier will be greater than it otherwise would be if that barrier were not present. In this case, hydraulic head measurements taken during pumping would not detect the presence of the barrier. Other methods available for locating impermeable barriers rely on datasets that can be clustered around the site of extraction rather than in the broader region (Cook et al. 2016), and so a barrier may remain undetected.

The role that groundwater barriers play in pumping test analysis has been thoroughly characterised (Ferris et al. 1962; Kruseman and de Ridder 2000; Pujades et al. 2012; Wu et. al 2017). In addition, methods have been developed for groundwater modelling in regions with hydraulic barriers, including: using analytical models (Fitts 1997); understanding horizontal (Anderson 2006) and vertical (Anderson and Bakker 2008) anisotropy across impermeable barriers, including in multi-aquifer settings; incorporating impermeable barriers into numerical modelling codes (Hsieh and Freckleton 1993); and using numerical models to test different permeabilities of fault zones (Bense and Person 2006). However, many of the studies have been limited to steady-state flow and few discussed the recovery period

following pumping. Yet predictions of groundwater levels in transient systems, including during groundwater recovery, are often required for the purpose of watershed and ecosystem management (Toran and Bradbury 1988; Currell et al. 2017).

If a barrier is undetected, and therefore not included in a conceptual model of a site, it can introduce structural uncertainty in model predictions. In general, the implications of structural model uncertainty have been well documented (Beven 2005; Bredehoeft 2005; Gupta et al. 2012; Refsgaard et al. 2012). However, to date no research has quantified the degree to which model predictions could be inaccurate if impermeable barriers are not included in models of groundwater drawdown. The aim of this study was therefore to determine both spatially and temporally when impermeable barriers should be considered in predictive groundwater models, and what their impact on groundwater level predictions could be.

Mathematical development

Analytical models (Theis 1935; Ferris et al. 1962) were used to compare groundwater drawdown with and without an impermeable barrier. The difference in drawdown between these two end members will be referred to as 'the effect of the barrier(s)'. The effect of a barrier, or multiple barriers, was evaluated during extraction (pumping phase) and also once pumping had ceased (recovery phase) at various distances from pumping and in aquifers with different geological properties. Drawdown from a pumping well was represented by the Theis equation (Theis 1935). For an aquifer of infinite extent and with a constant transmissivity, drawdown during pumping in a homogeneous aquifer (s_1^p) is represented as:

$$s_1^p = -\frac{Q}{4\pi T}\left(\mathrm{Ei}\left(\frac{-r^2}{4\kappa t}\right)\right) \quad (1)$$

Symbols are defined in Table 1, and Ei() represents the exponential integral function:

$$\mathrm{Ei}(x) = -\int_{-x}^{\infty} \frac{e^{-u}}{u}\, du \qquad (2)$$

Table 1 Description of symbols and dimensions

Symbol	*Description*
s_1^p	Drawdown [L] without a hydraulic barrier during pumping, where s > 0 indicates a lower hydraulic head.
s_2^p	Drawdown [L] with a hydraulic barrier during pumping.
s_1^r	Drawdown [L] without a hydraulic barrier during recovery.
s_2^r	Drawdown [L] with a hydraulic barrier during recovery.
Q	Extraction/pumping rate, where Q > 0 indicates extraction [L^3/T].
K	Hydraulic conductivity of aquifer [L/T].
b	Thickness of aquifer [L].
T	Transmissivity of aquifer [L^2/T].
S	Specific storage [dimensionless].
κ	Aquifer diffusivity = T/S [L^2/T].
r	Radial distance of the pumping well to the observation well/point [L].

R	Radial distance of the image well to the observation well/point [L].
L	Radial distance of the pumping well to the barrier [L].
t	Time at which drawdown is evaluated [T].
τ_{off}	Time at which pumping ceases, i.e. $Q = 0$ [T].
Δs^p	Difference in drawdown with and without the barrier: i.e. the effect of the barrier, during pumping [L].
Δs^r	Difference in drawdown with and without the barrier: i.e. the effect of the barrier, during recovery [L].
ϵ	The ratio of the maximum effect of the barrier during recovery compared to pumping.
t^r_{max}	Time of the maximum effect of the barrier during recovery [T].
Δs^{p*}	Non-dimensional difference in drawdown during pumping, where Δs^p [L] is scaled by $\frac{Q}{4\pi T}$ [L].

Δs^{r*}	Non-dimensional difference in drawdown during recovery, where Δs^r [L] is scaled by $\frac{Q}{4\pi T}$ [L].
r^{2*}	Non-dimensional distance from a pumping well to an observation well/point, where r^2 [L^2], is scaled by $4\kappa\tau_{off}$ [L^2].

Drawdown with an impermeable barrier, which is a no-flow boundary, for an observation well some distance, *r*, from the pumping well, can be derived by applying the superposition principle using the image well technique (Ferris et al. 1962), which assumes that the barrier has no permeability, spans the whole thickness of the aquifer and is of infinite length. A plan view schematic diagram of the problem is presented in Figure 1.

Drawdown at the observation well, in the presence of the impermeable barrier, can therefore be represented by:

$$s_2^p = -\frac{Q}{4\pi T}\left(\mathrm{Ei}\left(\frac{-r^2}{4\kappa t}\right) + \mathrm{Ei}\left(\frac{-R^2}{4\kappa t}\right)\right) \quad (3)$$

In this approach, *R* can be calculated if the angle, θ, between the line perpendicular to the barrier that passes through the pumping well and the line from the pumping well to the observation well is known, where $R = r \sin \boldsymbol{\theta} \sqrt{1+\left(\frac{2L-r\cos\theta}{r\sin\theta}\right)^2}$. Suppose that pumping ceases at a time $t = \tau_{off}$. Drawdown at the observation well for $t > \tau_{off}$ with no impermeable barrier present (s_1^r) is shown in Equation 4, and with a barrier present (s_2^r) is shown by Equation 5. These equations are obtained from Equations 1 and 3 by adding an additional expression for drawdown which uses an inflow term with the same, yet negative, rate of extraction *Q* where inflow begins at the cessation of pumping (where $t = \tau_{off}$). By the principle of superposition,

this is then added to the original drawdown for each time step, which results in water level simulations for the recovery period $t > \tau_{off}$.

$$s_1^r = -\frac{Q}{4\pi T}\left(\mathrm{Ei}\left(\frac{-r^2}{4\kappa t}\right)\right) + \frac{Q}{4\pi T}\left(\mathrm{Ei}\left(\frac{-r^2}{4\kappa(t-\tau_{off})}\right)\right) \quad (4)$$

$$s_2^r = -\frac{Q}{4\pi T}\left(\mathrm{Ei}\left(\frac{-r^2}{4\kappa t}\right) + \mathrm{Ei}\left(\frac{-R^2}{4\kappa t}\right)\right) + \frac{Q}{4\pi T}\left(\mathrm{Ei}\left(\frac{-r^2}{4\kappa(t-\tau_{off})}\right) + \mathrm{Ei}\left(\frac{-R^2}{4\kappa(t-\tau_{off})}\right)\right) \quad (5)$$

To observe the effect of two barriers on groundwater drawdown, where the two barriers are orthogonal, drawdown at an observation point can be calculated by including more image wells. With two orthogonal barriers, the imaginary system includes three image wells and thus Equation 3 expands to become Equation 6. R_{i1}, R_{i2} and R_{i3} represent the radial distances from the observation well to each of the image wells, *i1*, *i2* and *i3*, respectively (Figure 2). The drawdown in the observation well during pumping with two barriers is:

$$s_2^p = -\frac{Q}{4\pi T}\left(\mathrm{Ei}\left(\frac{-r^2}{4\kappa t}\right) + \mathrm{Ei}\left(\frac{-R_{i1}^2}{4\kappa t}\right) + \mathrm{Ei}\left(\frac{-R_{i2}^2}{4\kappa t}\right) + \mathrm{Ei}\left(\frac{-R_{i3}^2}{4\kappa t}\right)\right) \quad (6)$$

And drawdown in the observation well during recovery ($t > \tau_{off}$) with two barriers is:

$$s_2^r = -\frac{Q}{4\pi T}\left(\mathrm{Ei}\left(\frac{-r^2}{4\kappa t}\right) + \mathrm{Ei}\left(\frac{-R_{i1}^2}{4\kappa t}\right) + \mathrm{Ei}\left(\frac{-R_{i2}^2}{4\kappa t}\right) + \mathrm{Ei}\left(\frac{-R_{i3}^2}{4\kappa t}\right)\right) + \frac{Q}{4\pi T}\left(\mathrm{Ei}\left(\frac{-r^2}{4\kappa(t-\tau_{off})}\right) + \mathrm{Ei}\left(\frac{-R_{i1}^2}{4\kappa(t-\tau_{off})}\right) + \mathrm{Ei}\left(\frac{-R_{i2}^2}{4\kappa(t-\tau_{off})}\right) + \mathrm{Ei}\left(\frac{-R_{i3}^2}{4\kappa(t-\tau_{off})}\right)\right) \quad (7)$$

The difference in drawdown between the barrier and non-barrier scenarios (Δs) during pumping and recovery are:

$$\Delta s^p = s_2^p - s_1^p \quad (8)$$

$$\Delta s^r = s_2^r - s_1^r \quad (9)$$

Δs represents the effect of the barrier, and the error in a prediction of drawdown, where it may be uncertain whether or not a barrier is present. The time of the maximum effect of the barrier during pumping is the time at which pumping ceases because the effect of the barrier increases as drawdown increases. On the other hand, the time of the maximum effect of the barrier during recovery, t^r_{max}, will vary depending on pumping duration, τ_{off}, and aquifer diffusivity, κ. The value of t^r_{max}, for any value of τ_{off} where $t > \tau_{off}$, can be found by setting $\frac{d\Delta s^r}{dt} = 0$, and solving for t. For the one barrier case, this produces:

$$-\frac{\exp\left(-R^2/4\kappa t^r_{max}\right)}{t^r_{max}/\tau_{off}} + \frac{\exp\left(-R^2/4\kappa(t^r_{max}-\tau_{off})\right)}{\left(t^r_{max}/\tau_{off}\right)-1} = 0 \qquad (10)$$

or for the two orthogonal barrier case:

$$-\frac{\exp\left(-R_{i1}{}^2/4\kappa t^r_{max}\right)}{t^r_{max}/\tau_{off}} - \frac{\exp\left(-R_{i2}{}^2/4\kappa t^r_{max}\right)}{t^r_{max}/\tau_{off}} - \frac{\exp\left(-R_{i3}{}^2/4\kappa t^r_{max}\right)}{t^r_{max}/\tau_{off}} + \frac{\exp\left(-R_{i1}{}^2/4\kappa(t^r_{max}-\tau_{off})\right)}{\left(t^r_{max}/\tau_{off}\right)-1} +$$

$$\frac{\exp\left(-R_{i2}{}^2/4\kappa(t^r_{max}-\tau_{off})\right)}{\left(t^r_{max}/\tau_{off}\right)-1} + \frac{\exp\left(-R_{i3}{}^2/4\kappa(t^r_{max}-\tau_{off})\right)}{\left(t^r_{max}/\tau_{off}\right)-1} = 0 \qquad (11)$$

These can easily be solved numerically for t^r_{max}. It is also convenient to define the ratio of the maximum Δs^r to the maximum Δs^p:

$$\epsilon = \frac{max\Delta s^r}{max\Delta s^p} \qquad (12)$$

to understand the relative effect of the barrier during recovery compared to pumping. The $max\ \Delta s^p$ and $max\ \Delta s^r$ occur where $t = \tau_{off}$ and $t = t^r_{max}$, respectively. Where the effect of the barrier is high during recovery and low during pumping the value ϵ will be high. As the effect of the barrier during pumping approaches 0, the ratio approaches infinity.

Groundwater drawdown and recovery with a single barrier

Drawdown with and without an impermeable barrier during pumping and recovery was analysed over a wide parameter space initially for systems with one barrier (Equations 8 and 9). To study the circumstances where the effect of the barrier is not observed during pumping, yet is significant during recovery, $max\ \Delta s^p$ was compared to $max\ \Delta s^r$ for various values of r, κ and τ_{off} (Figure 3). To simplify, situations where $r = R = L$ were explored as this represents a worst-case scenario. This means that the observation well is at the point immediately adjacent to the barrier nearest the pumping well on the straight line between the pumping well and image well. Differences in drawdown Δs [L] are scaled by $\frac{Q}{4\pi T}$ [L] to give non-dimensional quantities Δs^*. The squared radial distance, r^2 [L^2], is scaled by $4\kappa\tau_{off}$ [L^2] to give the non-dimensional quantity r^{2*}. As the value of r^{2*} increases, the values of both $max\ \Delta s^{p*}$ and $max\ \Delta s^{r*}$ decrease, with $max\ \Delta s^{p*}$ always lower than $max\ \Delta s^{r*}$.

To understand the results, we can study the distance, r^{2*}, at which the effect of the barrier becomes insignificant (and therefore unobservable) in the pumping phase. Suppose that we define a significant amount of additional drawdown due to the presence of a barrier as $\Delta s > 1$ m. We consider three scenarios: $Q/T = 10^2$, 10^3 and 10^4 m, which respectively give $max\ \Delta s^{p*} = 0.13$, 0.013 and 0.0013. For each of these values, the largest value of $max\ \Delta s^{r*}$ (and hence also $max\ \Delta s^r$) can be determined each corresponding value of r^{2*}. From Figure 3, we therefore get r^{2*} values of 1.4, 3.0, and 4.9 for $Q/T = 10^2$ m, 10^3 and 10^4 m, respectively. For each distance, r^{2*}, the value of $max\ \Delta s^{r*}$ can therefore also be read from the graph. These non-dimensional values are, respectively, 0.27, 0.12 and 0.08, giving dimensional values for $max\ \Delta s^r$ of 2 m, 10 m and 59 m (for $Q/T = 10^2$ m, 10^3 m and 10^4 m).

Following a similar approach, we can explore the range of distances between which the effect of the barrier during pumping is not significant, but the barrier is not too far away—so that its effect during recovery is significant ($max\ \Delta s^p \leq 1$ m yet $max\ \Delta s^r \geq 1$ m). We refer to these

barriers as 'undetected' as hydraulic head measurements taken during pumping are not useful to predict recovery drawdown. From Figure 3, these are: $1.4 \leq r^{2*} \leq 2.9$, $3.0 \leq r^{2*} \leq 29$, $4.9 \leq r^{2*} \leq 91$ for $Q/T = 10^2$ m, 10^3 and 10^4 m, respectively. For a system with $\kappa = 500$ m^2/day and $\tau_{off} = 10$ years, these non-dimensional values of r^{2*} equate, respectively, to r values of 3140–4620 m, 4700–14,630 m, and 5990–25,800 m. Within these ranges of distance, ϵ respectively spans 2.0–8.7; 10.0–2.0 x 10^{12} and 59.0–4.5 x 10^{38} (Figure 4). This illustrates that the effect of the barrier during recovery is considerably greater than the effect of the barrier during pumping. However, as demonstrated, to determine the significance of the effect of the barrier during recovery one cannot simply refer to ϵ. This is because at high values of ϵ, the actual difference in drawdown induced by the barrier may be minor even if the ratio is large (as $max\ \Delta s^p$ approaches zero).

To exemplify the method and results, we analyse a hypothetical but realistic mining project that exists within a regional aquifer in which there is an observation well (say, at the site of a valued ecosystem) located on the pumping well side of a barrier 3 km away from the pumping well (see Figure 1 where $r = R = L = 3000$ m). The barrier has not been identified prior to the commencement of the project. Let us assume that dewatering proceeds for 10 years ($\tau_{off} = 3650$ days) where $Q = 10^5$ m^3/day (this rate of dewatering is known to occur at large open pit mines, Cook et al. 2016). The other aquifer properties are $K = 0.04$ m/day, $S = 0.1$, $b = 300$ m ($\kappa = 120$ m^2/day); giving $r^{2*} = 5$. Although the drawdown at the observation well during pumping is small, residual drawdown during the recovery phase is significant (Figure 5). The maximum effect of the barrier during the pumping period, $max\ \Delta s^p$, equals 0.7 m, and so the presence of the barrier is unlikely to be detected during pumping. After pumping ceases, as the extent of drawdown reaches the barrier, the residual drawdown curves for the barrier and the non-barrier model results diverge. The barrier-case residual drawdown curve is steeper than the non-barrier curve, as the barrier compartmentalises the aquifer and

less water is available on the pumping side of the barrier for water level recovery. During the recovery phase, the maximum difference between the barrier and non-barrier model results ($max\ \Delta s^r$) is 47 m observed at a t^r_{max} of 20,693 days (56 years), which is 46 years after the cessation of pumping. The value of ϵ for this example is 67, as the maximum effect of the barrier is considerably greater during recovery than during pumping, which highlights the importance of identifying barriers through other methods, such as hydrogeological mapping and geophysics, as their impact on water levels is delayed beyond the cessation of pumping.

Timing of the maximum effect of a barrier

The solution to Equation 10 for $r = R = L$ enables the comparison of the ratio of t^r_{max} to τ_{off} with r^{2*} (Figure 6). This shows when the maximum effect of the barrier in recovery will occur, compared to the total duration of pumping. As r^{2*} increases, t^r_{max} increases with respect to τ_{off}. As r^{2*} decreases, t^r_{max}/τ_{off} decreases and approaches 1. For $max\ \Delta s^p$ = 1 m, and Q/T = 10^2 m, 10^3 and 10^4 m, t^r_{max}/τ_{off} = 2.0, 3.6 and 5.5, respectively. This means that, say for a groundwater extraction project that extends for 10 years (τ_{off} = 10 years), the greatest effects of the barrier will not be until 10, 26 or 45 years after pumping ceases for these values of Q/T.

Groundwater drawdown and recovery with two orthogonal barriers

If there is more than one impermeable barrier, the effect of the barriers on drawdown will be greater than in the single barrier case, as the aquifer becomes more compartmentalised. We study the effect of two orthogonal barriers, with an observation well located on the pumping side of the junction of these barriers, as a case study to exemplify highly compartmentalised systems. In this case, the radial distance from each of the real or imaginary discharging wells will be equal ($r = R_{i1} = R_{i2} = R_{i3}$). Under this assumption, Equation 6 simplifies to Equation 13, and Equation 7 simplifies to Equation 14.

$$s_2^p = -\frac{Q}{4\pi T}\left(4\ \mathrm{Ei}\left(\frac{r^2}{4\kappa t}\right)\right) \quad (13)$$

$$s_2^r = -\frac{Q}{4\pi T}\left(4\ \mathrm{Ei}\left(\frac{-r^2}{4\kappa t}\right)\right) + \frac{Q}{4\pi T}\left(4\ \mathrm{Ei}\left(\frac{-r^2}{4\kappa(t-\tau_{off})}\right)\right) \quad (14)$$

Note that in this case, as the observation well is immediately adjacent to the junction of the two barriers, $r \neq L$, and thus the barriers are each closer to the pumping well than in the one barrier scenario. Therefore, in this case r represents the distance to *both* barriers, where they intersect, so in the two barrier scenario: $L_1 = L_2 = \sqrt{r^2/2}$. During both pumping and recovery, $max\ \Delta s^*$ decreases with increasing r^{2*}. In comparison to the one barrier solution, overall the values are higher (Figure 7). The values of r^{2*}, for which $max\ \Delta s^p \leq 1$ m, and $max\ \Delta s^r \geq 1$ m, are $2.1 \leq r^{2*} \leq 8.8$, $3.9 \leq r^{2*} \leq 59$ and $5.9 \leq r^{2*} \leq 127$ for $Q/T = 10^2$, 10^3 and 10^4 m, respectively. Respective values of ϵ are 4–2.6 x 10^3, 22–7.6 x 10^{24} and 149–1.9 x 10^{51}, which can be found using the results for the one barrier case (Figure 4), as the ratio $max\Delta s^r/max\Delta s^p$ compared to r^{2*} is the same for both case studies. In the two orthogonal barrier case, the values of $max\ \Delta s^r$ (for $max\ \Delta s^p = 1$ m) are 4 m, 22 m and 149 m.

To determine the timing of the maximum effect of the impermeable barrier, where $r = R_{i1} = R_{i2} = R_{i3}$, and for $t > \tau_{off}$, Equation 11 simplifies to become the same as Equation 10 and the value of t^r_{max} can be determined using Figure 5. For the three values of Q/T described earlier, at $max\ \Delta s^r$, where $max\ \Delta s^p = 1$ m: $t^r_{max}/\tau_{off} = 2.7$; $t^r_{max}/\tau_{off} = 4.5$; and $t^r_{max}/\tau_{off} = 6.4$, respectively. This shows that for a groundwater extraction project that extends for 10 years ($\tau_{off} = 10$ years), the effect of the barriers will be greatest at 17, 35 or 54 years after pumping ceases if $Q/T = 10^2$ m; $Q/T = 10^3$ m or $Q/T = 10^4$ m, respectively.

Maximum error in predictions of hydraulic head during recovery

It is also useful to understand: (a) how large the effect of an undetected barrier could be in recovery for any given Q/T and (b) the distances, r, for which this phenomenon may be observed with respect to aquifer and pumping properties. To do this, for each value of Q/T, we can find the value of $max\ \Delta s^{p*}$ where $max\ \Delta s^{p} = 1$ m. From this we can derive the corresponding value of r^{2*} (Figure 3 or Figure 7), and thus also $max\ \Delta s^{r*}$ and hence Δs^{r}. This is shown in Figure 8. As Q/T increases, so do $max\ \Delta s^{r}$ and r^{2*}. For values of Q/T between 1–10^4 m, the non-dimensional values of r^{2*} that results in $max\ \Delta s^{p} = 1$ m range between 0.01–10. The dimensional values of r can be derived by dividing r^{2*} by a specific value of $4\kappa\tau_{off}$. For example, if $Q/T = 10^2$ m, for values of $\kappa\tau_{off}$ between 10^6–10^8 m^2, r ranges between 10^3 and 10^5 m.

Discussion and conclusions

This paper shows that in areas with impermeable barriers, hydraulic head measurements made during pumping cannot reliably be used to predict recovery. This can occur if impermeable barrier(s) exists outside the extent of drawdown induced during pumping. The results indicate that, for an observation well located 3 km from a pumping project, the effect of a barrier on groundwater levels can be less than 1 m during pumping, yet almost 50 m after pumping has ceased. The timing of the maximum effect of a barrier on groundwater levels is proportional to the duration of pumping and will increase as the distance of the barrier from a pumping project increases.

The results were based on analytical models that used the linearised Boussinesq equations (Dupuit assumption). Other assumptions include: that the hydraulic barrier is completely impermeable, of infinite length, fully penetrating and that the aquifer is homogeneous. Our model of hydraulic barriers is thus highly simplified, and does not consider the permeability structure associated with fault zones (Caine et al., 1996; Bense et al., 2013). We also do not

consider multi-aquifer systems in which faults create offsets on aquifer layers, or faults that act as barriers to perpendicular flow across the fault but as a conduits to flow in the vertical direction or along, parallel to, the fault. Steady state analytical models of these systems have been considered (Anderson 2006; Anderson et al. 2008). Further research into methods for modelling barriers with complex permeability and isotropy under transient conditions would be useful, where numerical modelling and field studies could complement the use of analytical or analytical-element models. The assumptions of zero permeability and isotropy across barriers in this paper allow for a worst-case assessment of omitting impermeable barriers from predictive models of groundwater levels based on hydraulic head measurements taken during pumping.

Where the effect of a barrier during pumping is insignificant, other methods are required to detect its presence. These might include surface or aerial geophysics (Ball et al. 2010; Vittecoq et al. 2015), geochemistry and environmental tracers (Pereira et al. 2010; Rajabpour and Vaezihir 2016; Sun et al. 2018; Toutain and Baubron 1999; Umeda and Ninomiya 2009), and lineament analysis (Sander et al. 1997; Tam et al. 2004). Analysis of the pre-pumping potentiometric surface might also provide information on the existence of barriers to flow (Bense et al. 2003; Seaton and Burbey 2005), although often bore networks are sparse in areas that are not affected by groundwater pumping. This is certainly the case in northwest Australia, where dewatering of large open pit mines occurs in areas of highly complex geology (Cook et al., 2016). Nevertheless, the use of multiple data sets, such as geochemistry, temperature and hydraulic heads, can shed light on past and current groundwater dynamics in regions impacted by pumping (Gumm et al. 2016). However, interpreting variations in hydraulic conductivity and geological structures from some methods can be challenging (e.g. Viezzoli et al. 2013). Therefore, simple approaches to understand the impact of impermeable barriers on predictions of future groundwater levels can be very useful.

Acknowledgements

This work was undertaken as part of a collaborative project between the National Centre for Groundwater Research and Training (NCGRT) and Rio Tinto Iron Ore. Funding was provided by the Australian Government Research Training Program, the Australian Research Council, through Linkage Grant LP150100395 and by Rio Tinto Iron Ore. We appreciate the feedback provided by Matthew Currell and two anonymous reviewers, which improved the manuscript. Many thanks go to Saskia Noorduijn, James McCallum and Leonard Konikow for their ideas and suggestions. The corresponding author is grateful to the United States Geological Survey for hosting her as a visiting researcher.

References

Allen, D. M. and F. A. Michel. 1999. Characterizing a Faulted Aquifer by Field Testing and Numerical Simulation. *Groundwater* 37, no. 37: 718–728.

Anderson, E. I. 2006. Analytical solutions for flow to a well through a fault. *Advances in Water Resources* 29: 1790–1803.

Anderson, E. I. and M. Bakker. 2008. Groundwater flow through anisotropic fault zones in multiaqufier systems. *Water Resources Research* 44: 1–11.

Babiker, M. and A. Gudmundsson. 2004. The effect of dykes and faults on groundwater flow in an arid land: the Red Sea Hills, Sudan. *Journal of Hydrology* 297: 256–273.

Ball, L. B., S. Ge, J. S. Caine, A. Revil, and A. Jardani. 2010. Constraining fault-zone hydrogeology through integrated hydrological and geoelectrical analysis. *Hydrogeology Journal* 18: 1057–1067.

Bense, V. F., R. T. Van Balen, and J. J. De Vries, 2003. The impact of faults on the hydrogeological conditions in the Roer Valley Rift System: an overview. *Netherlands Journal of Geosciences* 82, no. 1: 42–54.

Bense, V. F., and M. A. Person. 2006. Faults as conduit-barrier systems to fluid flow in siliciclastic sedimentary aquifers. *Water Resources Research* 42, no. 42: 1–18.

Bense, V. F., T. Gleeson, S. E. Loveless, O. Bour, and J. Scibek. 2013. Fault zone hydrogeology. *Earth-Science Reviews* 127: 171–192.

Bense, V. F., and R. Van Balen. 2004. The effect of fault relay and clay smearing on groundwater flow patterns in the Lower Rhine Embayment. *Basin Research* 16: 397–411.

Beven, K., 2005. On the concept of model structural error. *Water Science and Technology* 52, no. 6: 167–175.

Bredehoeft, J. D. 2005. The conceptualization model problem—surprise. *Hydrogeology Journal* 13: 37–46.

Bredehoeft, J. D. 2011. Monitoring Regional Groundwater Extraction: The Problem. *Groundwater* 49, no. 6: 808–814.

Caine, J. S., J. P. Evans, and C. B. Forster. 1996. Fault zone architecture and permeability structure. *Geology* 24, no. 11: 1025–1028.

Cook, P. G., S. Dogramaci, J. L. McCallum, and J. Hedley. 2016. Groundwater age, mixing and flow rates in the vicinity of large open pit mines, Pilbara region, northwestern Australia. *Hydrogeology Journal* 25, no. 1: 39–53.

Currell, M. J., A. D. Werner, C. McGrath, J. A. Webb, and M. Berkman. 2017. Problems with the application of hydrogeological science to regulation of Australian mining

projects: Carmichael Mine and Doongmabulla Springs. *Journal of Hydrology*, 548: 674–682.

Ferris, J. G., D. B. Knowles, R. H. Brown, and R. W. Stallman. 1962. Theory of aquifer tests. U.S. Geological Survey Water-Supply Paper 1536–E. U.S. Washington D.C.: Department of the Interior, United States Government Printing Office.

Fitts, C. R. 1997. Analytic Modeling of Impermeable and Resistant Barriers. *Groundwater* 35, no. 2: 312–317.

Gumm, L. P., V. F. Bense, P. F. Dennis, K. M. Hiscock, N. Cremer, and S. Simon. 2016. Dissolved noble gases and stable isotopes as tracers of preferential fluid flow along faults in the Lower Rhine Embayment, Germany. *Hydrogeology Journal* 24: 99–108.

Gupta, H. V., M. P. Clark, J. A. Vrugt, G. Abramowitz, and M. Ye. 2012. Towards a comprehensive assessment of model structural adequacy. *Water Resources Research* 48: 1–16.

Hsieh, P. A. and J. R. Freckleton, 1993. Documentation of a computer program to simulate horizontal-flow barriers using the U.S. Geological Survey modular three-dimensional finite difference ground-water flow model. Open-File Report 92-477. Denver, Colorado: USGS.

Kruseman, G. P., and N. A. de Ridder. 2000. Analysis and Evaluation of Pumping Test Data. Second Edition (Completely Revised). The Netherlands: International Institute for Land Reclamation and Improvement.

Mayer, A., W. May, C. Lukkarila, and J. Diehl. 2007. Estimation of fault-zone conductance by calibration of a regional groundwater flow model: Desert Hot Springs, California. *Hydrogeology Journal* 15: 1093–1106.

Pereira, A. J. S. C., M. M. Godinho and L. J. P. F. Neves. 2010. On the influence of faulting on small-scale soil-gas radon variability: a case study in the Iberian Uranium Province. *Journal of Environmental Radioactivity* 101: 875–882.

Pujades, E., A. Lopez, J. Carrera, E. Vazquez-Sune, and A. Jurado. 2012. Barrier effect of underground structures on aquifers. *Engineering Geology* 145-146: 41–49.

Rajabpour, H. and A. Vaezihir. 2016. Hydrogeological Studies to Identify the Trend of Concealed Section of the North Tabriz Fault (Iran). *Groundwater* 55, no. 3: 327–333.

Rawling, G. C., L. B. Goodwin, and J. L. Wilson. 2001. Internal architecture, permeability structure, and hydrologic significance of contrasting fault-zone types. *Geology* 29, no. 1: 43–46.

Refsgaard, J. C., S. Christensen, T. O. Sonnenborg, D. Seifert, A. L. Højberg, and Troldborg, 2012. Review of strategies for handling geological uncertainty in groundwater flow and transport modelling. *Advances in Water Resources* 36: 36–50.

Sander, P., T. B. Minor, and M. M. Chesley. 1997. Ground-Water Exploration Based on Lineament Analysis and Reproducibility Tests. *Groundwater* 35: 888–894.

Seaton, W. J. and T. J. Burbey. 2005. Influence of Ancient Thrust Faults on the Hydrogeology of the Blue Ridge Province. *Groundwater* 44, no. 3: 301–313.

Sun, X., P. Yang, Y. Xiang, X. Si and D. Liu. 2018. Across-fault distributions of radon concentrations in soil gas for different tectonic environments. *Geosciences Journal* 22, no. 2: 227–239.

Tam, V. T., F. De Smedt, O. Batelaan, and A. Dassargues. 2004. Study on the relationship between lineaments and borehole specific capacity in a fractured and karstified limestone area in Vietnam. *Hydrogeology Journal* 12: 662–673.

Theis, C. V. 1935. The relation between the lowering of the Piezometric surface and the rate and duration of discharge of a well using ground-water storage. *Transactions American Geophysical Union* 16, no. 2: 519–524.

Toran, L. and K. R. Bradbury. 1988. Ground-Water Flow Model of Drawdown and Recovery Near an Underground Mine. *Groundwater* 26, no. 6: 724–733.

Toutain, J. and J. Baubron. 1999. Gas geochemistry and seismotectonics: a review. *Tectonophysics* 304: 1–27.

Umeda, K. and A. Ninomiya. 2009. Helium isotopes as a tool for detecting concealed active faults. *Geochemistry, Geophysics, Geosystems* 10, no. 8: 1–10.

Viezzoli, A., F. Jorgensen, and C. Sorensen. 2013. Flawed Processing of Airborne EM Data Affecting Hydrogeological Interpretation. *Groundwater* 51, no. 2: 191–202.

Vittecoq, B., P. A. Reninger, S. Violette, G. Martelet, B. Dewandel, and J. C. Audru. 2015. Heterogeneity of hydrodynamic properties and groundwater circulation of a coastal andesitic volcanic aquifer controlled by tectonic induced faults and rock fracturing – Martinique island (Lesser Antilles – FWI). *Journal of Hydrology* 529: 1041–1059.

Wu, Y., J. S. Shen, W. Cheng, and T. Hino. 2017. Semi-analytical solution to pumping test data with barrier, wellbore storage, and partial penetration effects. *Engineering Geology* 226: 44–51.

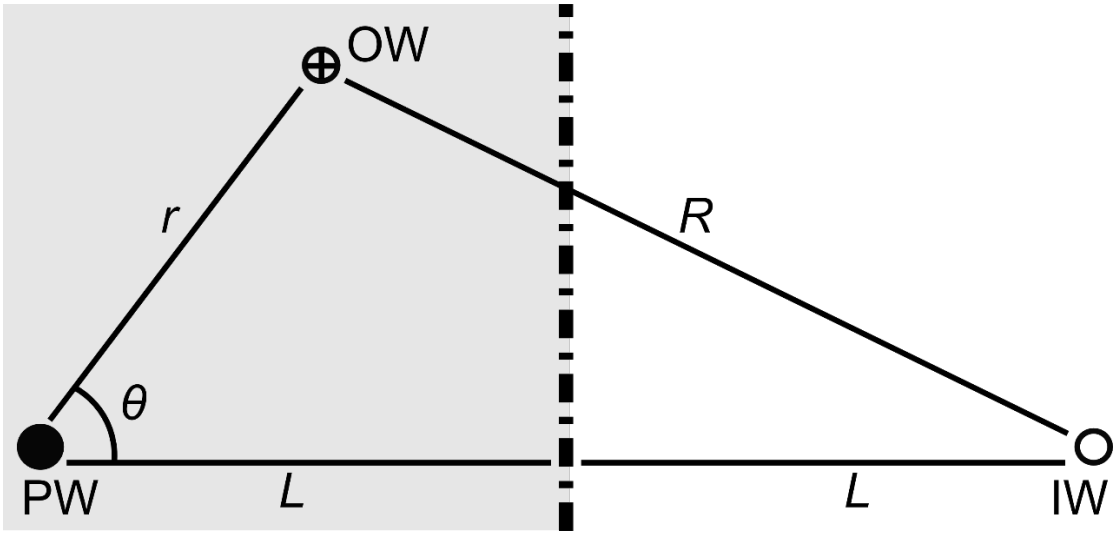

Figure 1. Schematic, plan-view diagram of notation used in the analytical method to calculate drawdown in the presence of an impermeable barrier (*dot-dash line*). The *shaded region* represents the physical region, the *white region* represents the imaginary region. The solution from an image well, depicted by the *open black circle*, was used along with real discharge at the pumping well, depicted by the *filled black circle*, to derive the solution for drawdown at the observation well shown as the *black circle filled with a cross*. *PW* = Pumping well; *OW* = Observation well; *IW* = Image well.

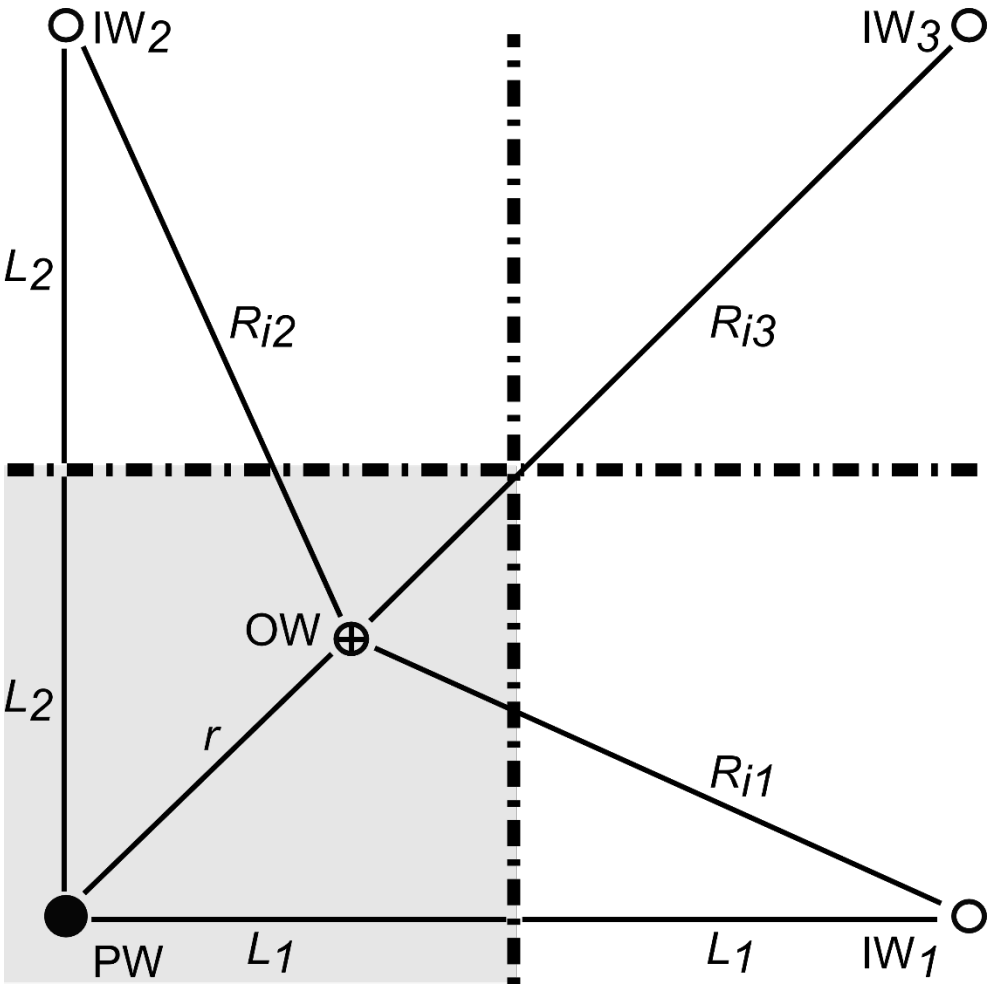

Figure 2. Schematic, plan-view diagram of notation used in the analytical method to calculate drawdown in the presence of a two hydraulic barriers (*dot-dash lines*). The *shaded region* represents the physical region, the *white region* represents the imaginary region. The solution from three image wells, IW_1, IW_2 and IW_3, depicted by *black open circles* were used along with real discharge at the pumping well, depicted by the *black filled circle*, to derive the solution for drawdown at the observation well shown as the *black circle filled with a cross*. *PW* = Pumping well; *OW* = Observation well; *IW* = Image well.

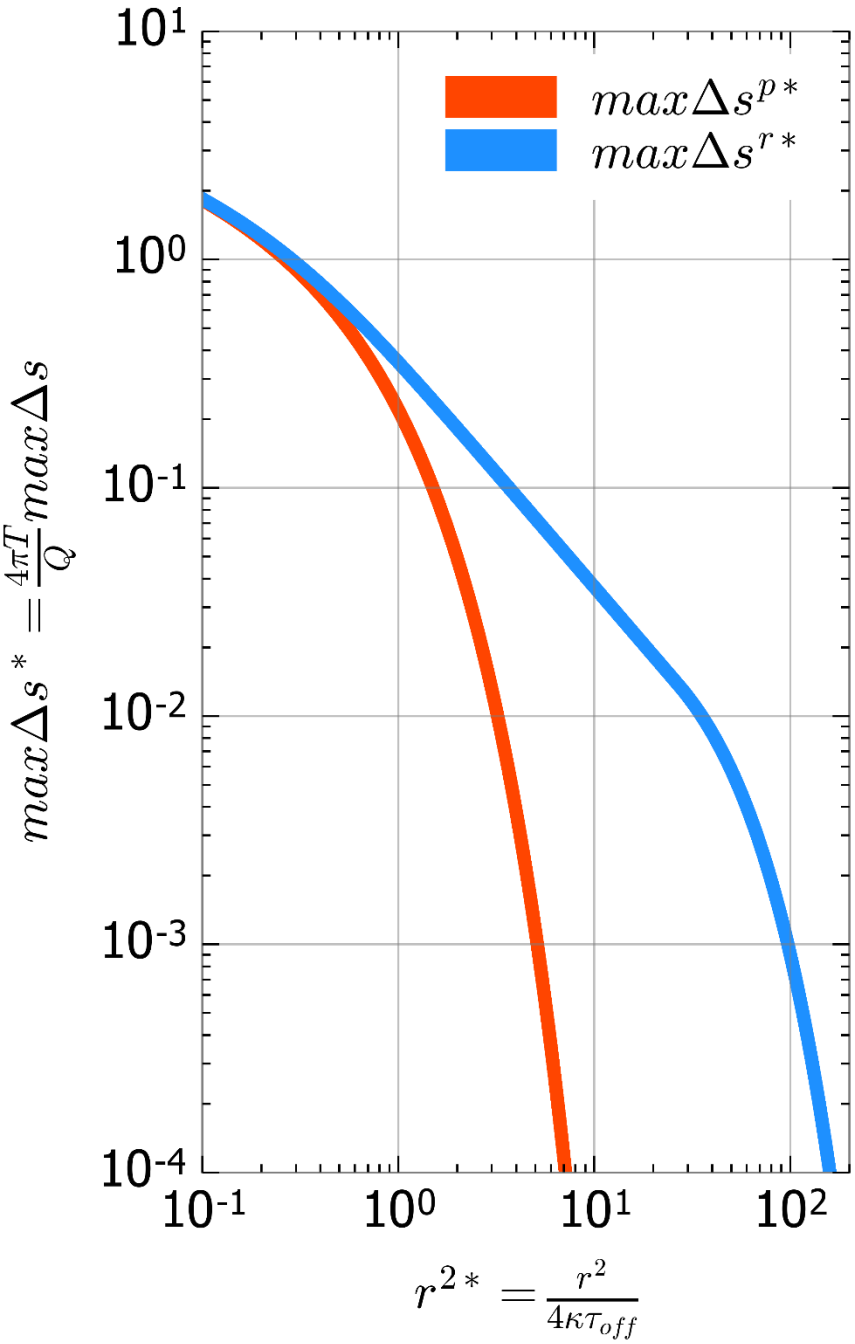

Figure 3. Generalised graph of maximum difference in drawdown between the one barrier case and the no barrier case during pumping (in *red*) and recovery (in *blue*), where $r = R = L$, as a function of non-dimensional distance (r^{2*}).

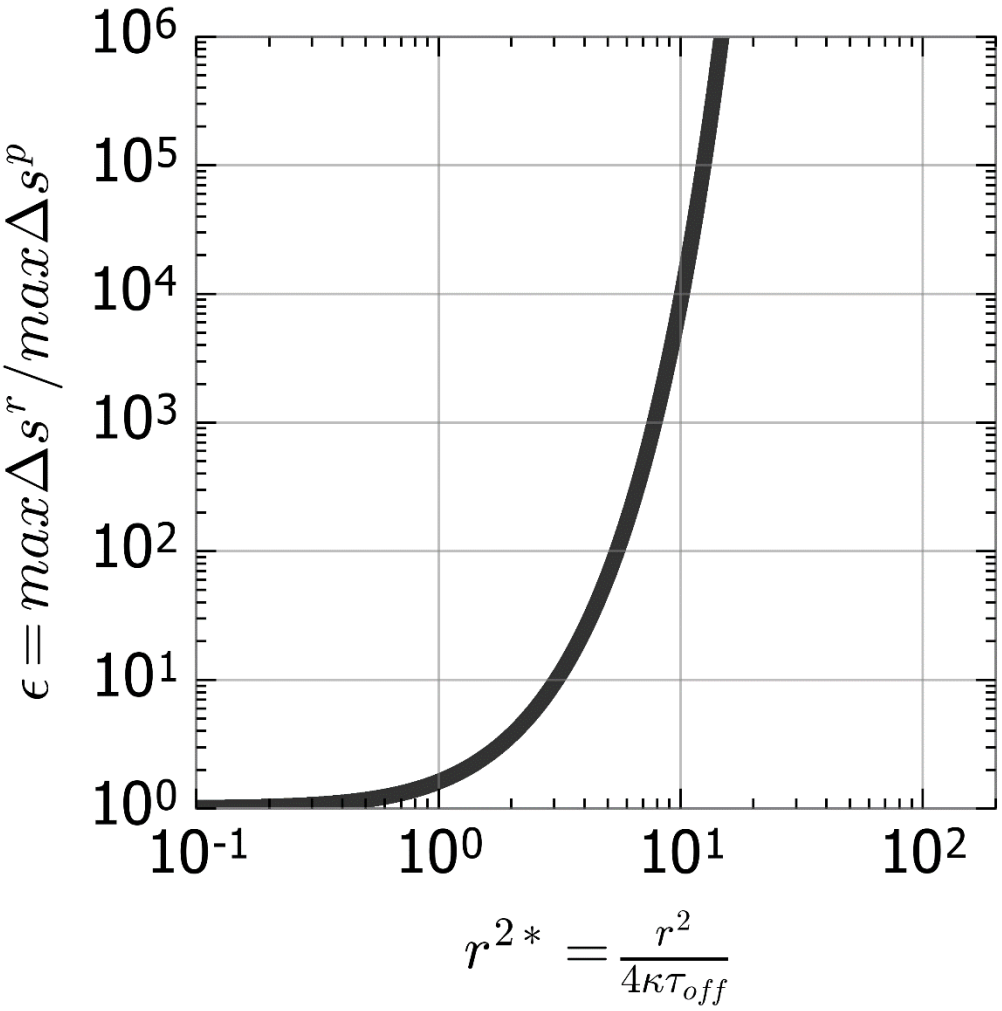

Figure 4. Generalised graph of the ratio of the maximum difference in drawdown between the barrier and no barrier case during pumping compared to recovery (ϵ), where $r = R = L$, as a function of r^{2*}.

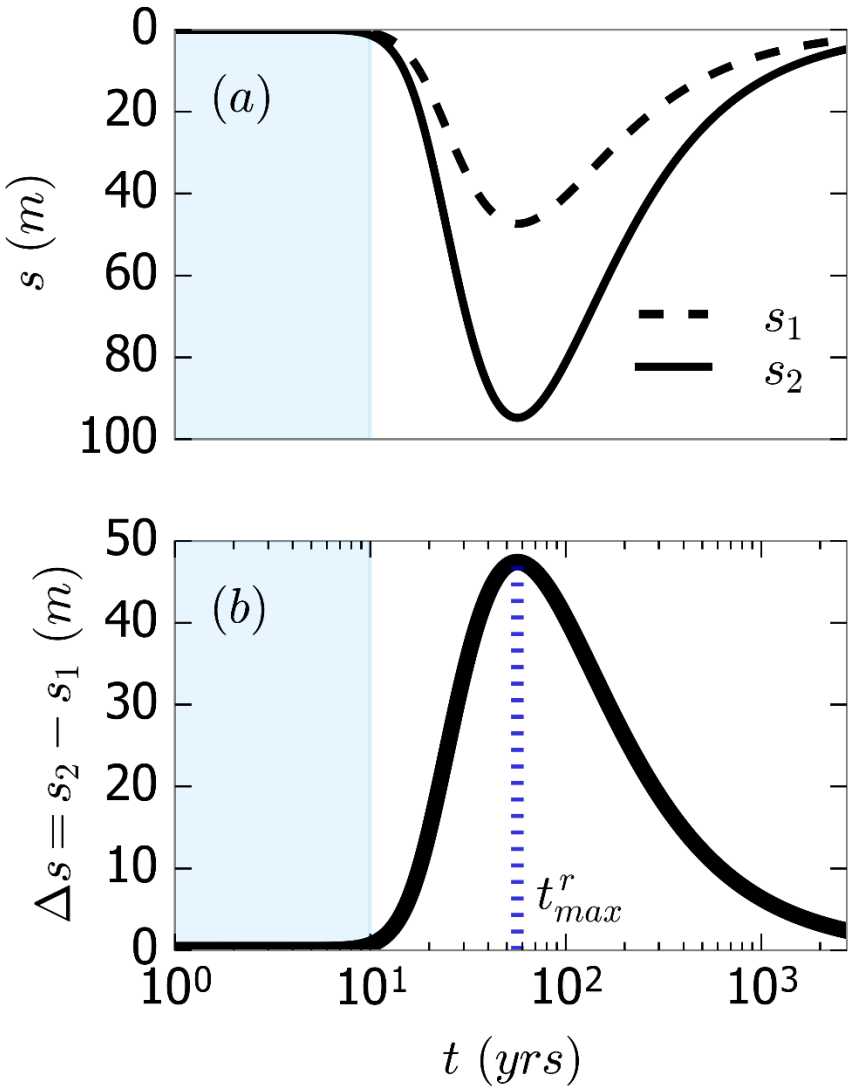

Figure 5. Results of analytical simulation of extraction and recovery for an aquifer 300 m thick, where $Q = 10^5$ m^3/days, $r = 3000$ m with $K = 0.04$ m/days ($T = 12$ m^2/days), and $S = 0.1$. The *blue shaded area* denotes the period of pumping, where $\tau_{off} = 10$ years. (a) Groundwater drawdown for the no barrier case (s_1) and the one barrier case (s_2); (b) the difference between drawdown with and without the barrier ($\Delta s = s_2 - s_1$). t^r_{max} is the time where Δs is the greatest, which occurs at 56 yrs.

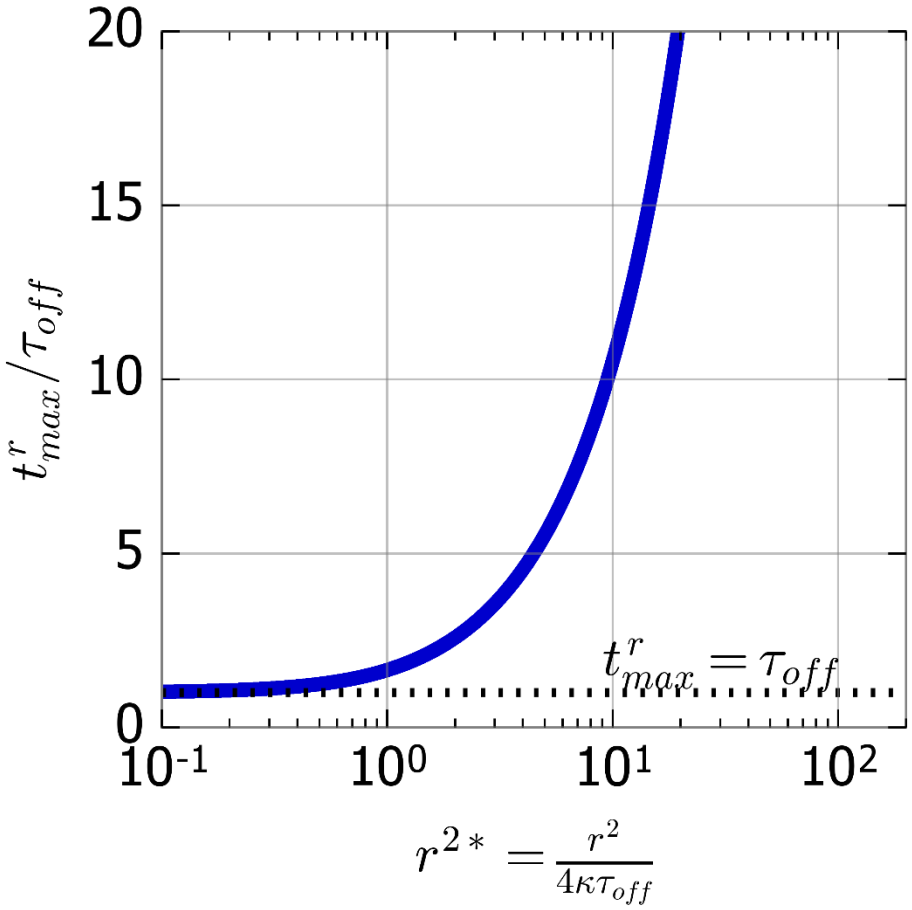

Figure 6. The time that the maximum effect of the barrier occurs (t^r_{max}) as a ratio to pumping duration (t^r_{max}/τ_{off}) compared to r^{2*}.

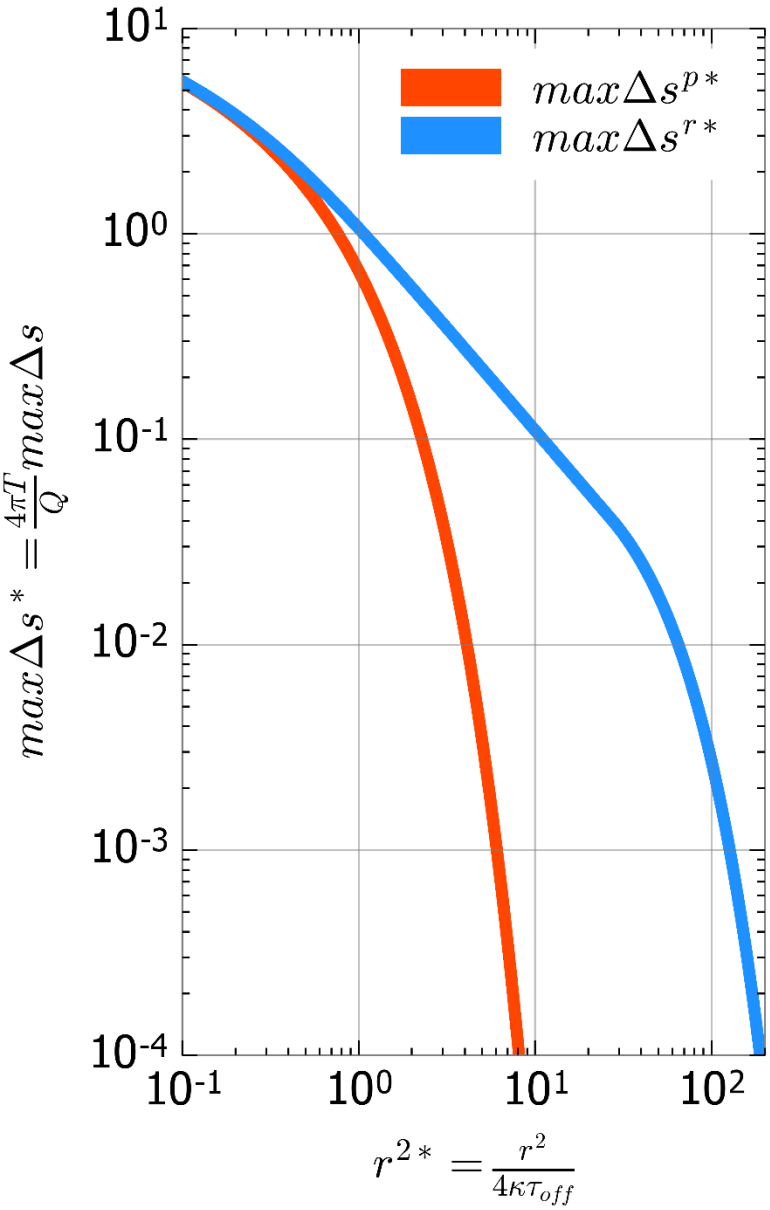

Figure 7. Generalised graph of maximum difference in drawdown between the two orthogonal barriers case and the no barrier case during pumping (in *red*) and recovery (in *blue*), where $r = R = L$, as a function of non-dimensional distance (r^{2*}).

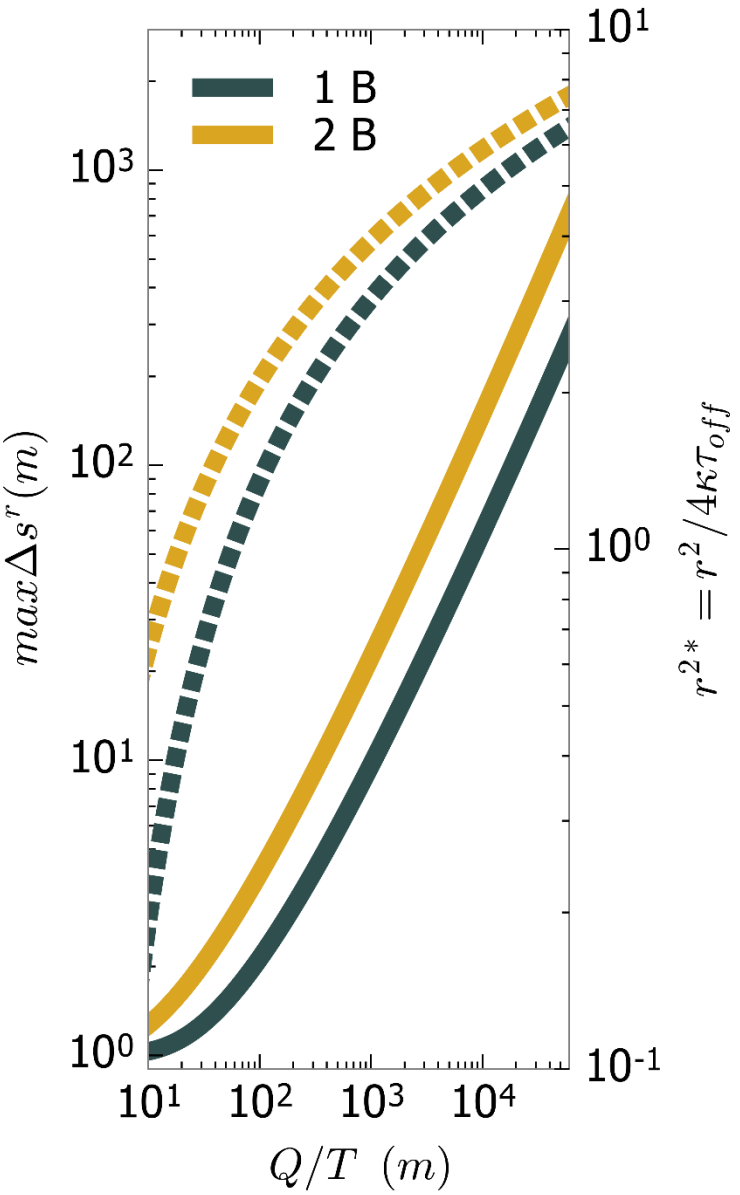

Figure 8. The value of *max* Δs^r for an undetected barrier, where Δs^p = 1 m, depending on the value of *Q/T* is shown by the *solid lines* for both the one barrier case (*1 B*) and two orthogonal barrier case (*2 B*). The r^{2*} corresponding to each *max* Δs^r value for a specific *Q/T* value is depicted with the *hashed lines*. These r^{2*} values can be used to calculate dimensional values of *r*, in metres, by dividing them by a specific value of $4\kappa\tau_{off}$.